Supplementary Material

Biopolymer Meets Nanoclay: Rational Fabrication of Superb Adsorption Beads From Green Precursors for Efficient Capture of Pb(II) and Dyes

Jie Qi,† Xue Wang,† Huan Zhang, Xiangyu Liu, Wenbo Wang, Qingdong He, Fang Guo*

College of Chemistry and Chemical Engineering, Inner Mongolia University, Hohhot 010021, China; jieino@163.com (J.Q.); 542446320@qq.com (X. W.); hzhang1989@163.com (H. Z.); lxy13257244737@163.com (X.L.); wangwenbo@imu.edu.cn (W.W.); 18847744604@163.com (Q.H.); guofang@imu.edu.cn (F. G.)

* Correspondence: guofang@imu.edu.cn (F.G.)

†These authors contribute equally to the paper.

Part I: Equations and characterizations

1.1 Equations

The experimental data were fitted with kinetic mathematical models: pseudo-first order kinetic model (Equation S1) and pseudo-second order kinetic models (Equation S2).

$$\frac{t}{q_t} = \frac{1}{k_2 q_e^2} + \frac{t}{q_e}$$

(S1)

$$\text{Log}(q_e - q_t) = \log q_e - \frac{k_1 t}{2.303}$$

(S2)

where q_t and q_e are the adsorption capacity at time t and at adsorption equilibrium, respectively (mg/g), k_1 (min⁻¹) and k_2 (g/(mg·min) are pseudo-first order and pseudo-second order kinetic constants [77].

The adsorption data were fitted with different adsorption isotherm models: Langmuir model (Equation S3) , Freundlich model(Equation S4) and Sips model (Equation S5) [78].

$$q_e = k_f C_e^{\frac{1}{n}} \tag{S3}$$

$$q_e = \frac{q_m k_L C_e}{1 + C_e k_L} \tag{S4}$$

$$q_e = \frac{k_s C_e^{\beta_s}}{1 + a_s C_e^{\beta_s}} \tag{S5}$$

where q_e is the adsorption capacity at adsorption equilibrium state (mg/g), q_m is the maximum adsorption capacity (mg/g); K_L is the Langmuir constant related to theoretical monolayer adsorption (L/mg); C_e is the concentration of adsorbate in solution at adsorption equilibrium state (mg/L); K_f is the Freundlich adsorption isotherm constant [(mg/L)(L/g) 1/n]; n is a constant related to the intensity of adsorption [79]. K_s is the Sips model isotherm constant (L/g); a_s the Sips model constant (L/mg) and β_s the Sips model exponent.

1.2 Characterizations

The surface morphologies of composite beads were examined using a Field Emission Scanning Electron microscope (SUPRA55, Carl Zeiss, Germany). The microscopic structure was observed with a high resolution transmission electron microscope (JEM-2100f, JEOL, Japan). Fourier transform infrared (FTIR) spectra were measured with a Nicolet iS10 spectrophotometer (Thermo Fisher, USA). The crystallization state of the composite beads with different clay content was analyzed by a X-ray powder diffractometer (D8 Advance, Bruker, Germany) equipped with a Cu-Kα radiation source (40 kV, 40 mA). X-ray photoelectron spectroscopy (XPS) was measured with an ESCALAB Xi+ spectrophotometer (Thermo Fisher Scientific, American). After adsorption process, the composite beads were removed from the solution, and the concentration of residual dye in the solution was tested with a UV1900i UV–Vis spectrophotometer (Shimadzu, Japan). Zeta potentials were tested with a NanoBrook 90Plus Zeta Potentiometer (Brookhaven, USA). The concentration of Pb(II) ions was measured with a ZEEnit 700P Atomic Absorption Spectrometer (Analytic Jena, Germany). The content of Na in SA was determined with an Avio 200 ICP instrument (Perking Elmer, USA).
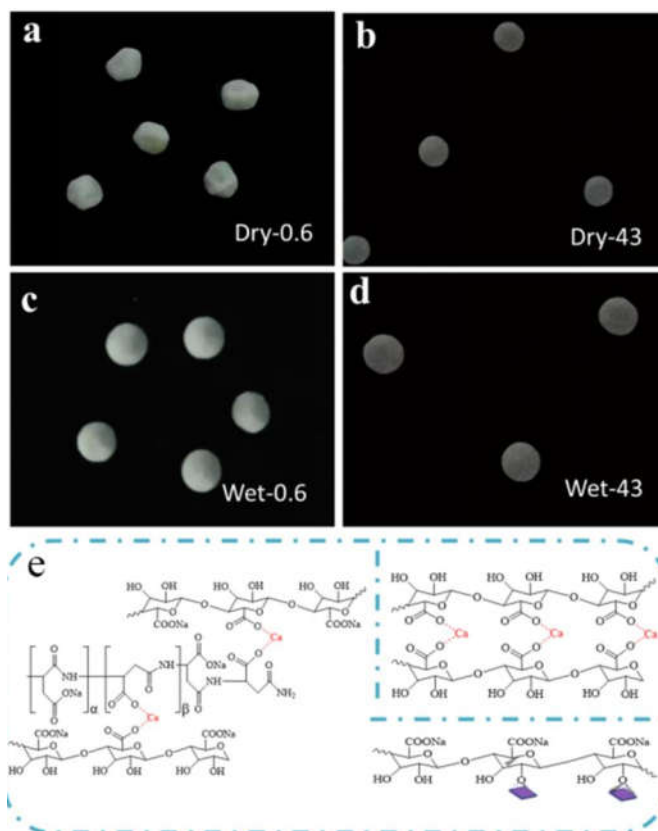
Part II. Supplementary Figures
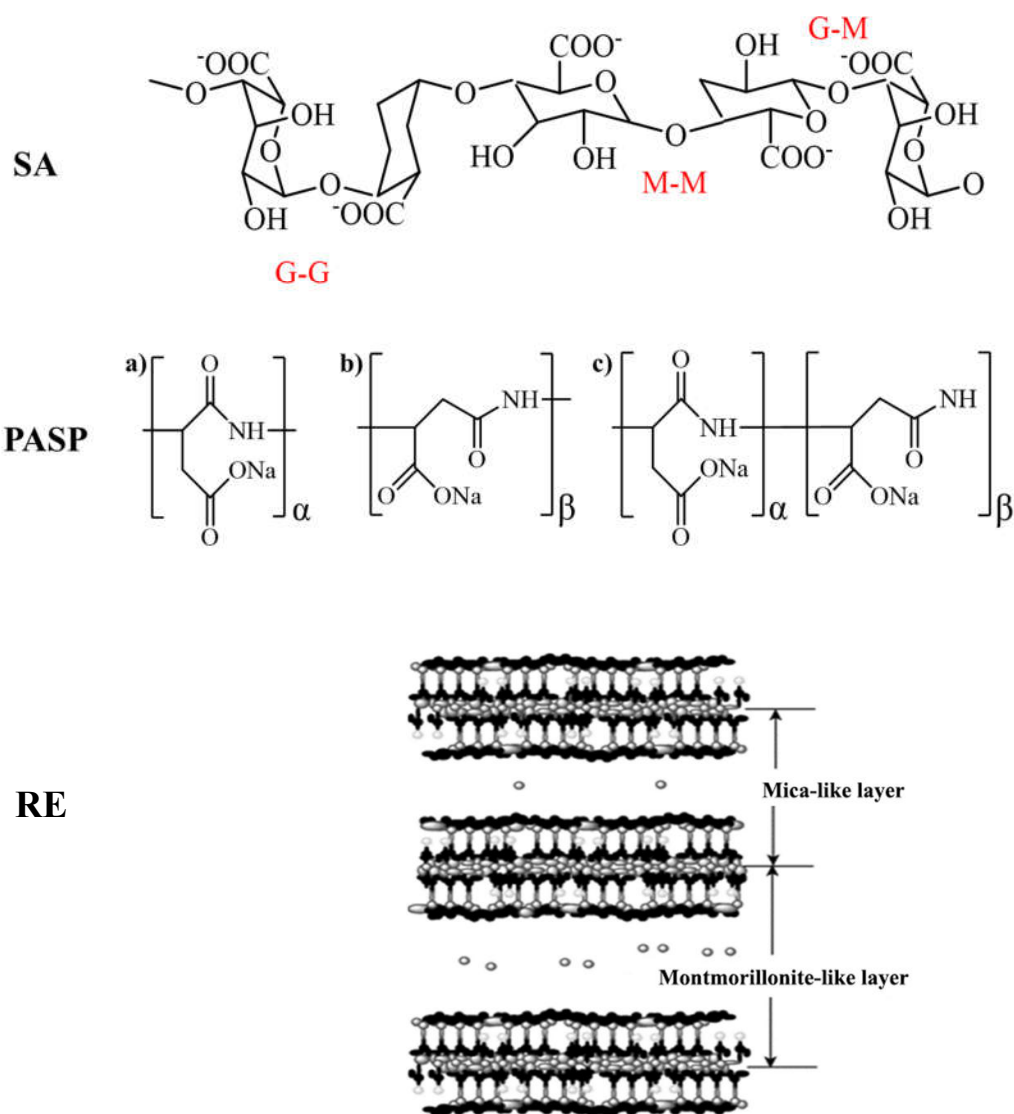
**Figure S1.** The structure scheme of SA, PASP, and RE [80].
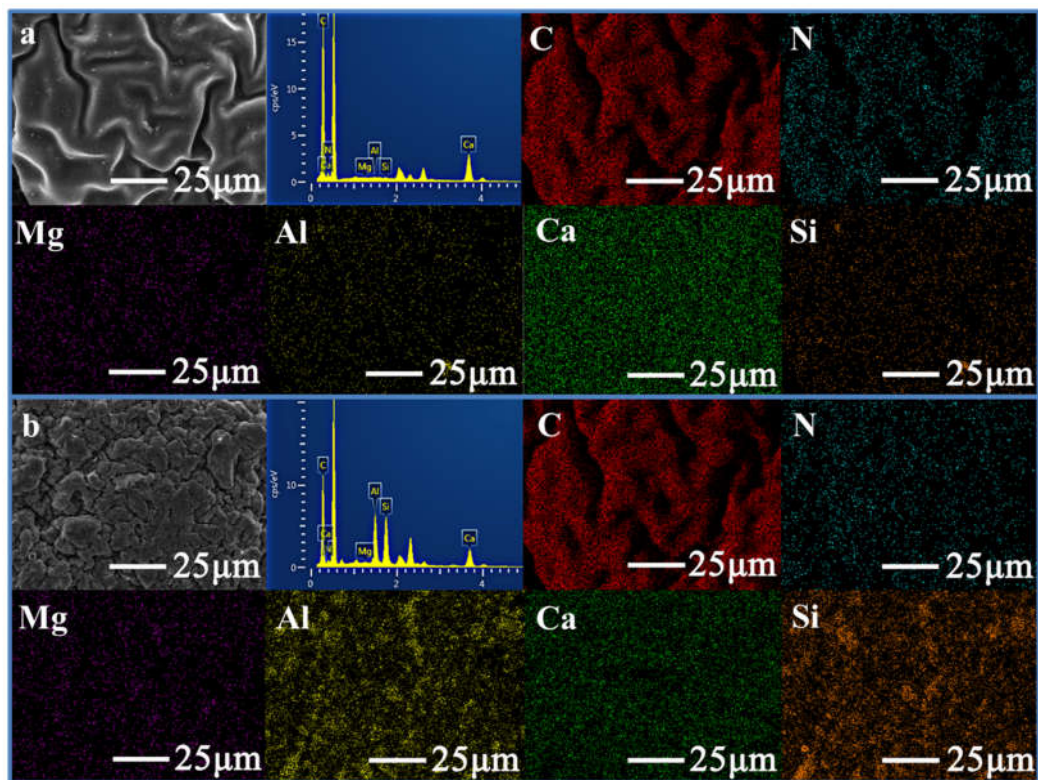
Figure S2. (a) SEM images, EDS curves and corresponding element mapping of C, N, Mg, Al, Ca, Si elements in SA/PASP/RE0.6; and (b) SEM image, EDS curves and corresponding element mapping of C, N, Mg, Al, Ca, Si elements in SA/PASP/RE43.

Figure S3. The digital photos of the SA/PASP/RE0.6 composite beads: (a) Dry state and (c) Wet-state; and the digital photos of the SA/PASP/RE43 composite beads: (b) Dry and (d) Wet-state; and (e) a scheme for the ion-crosslinking structure.
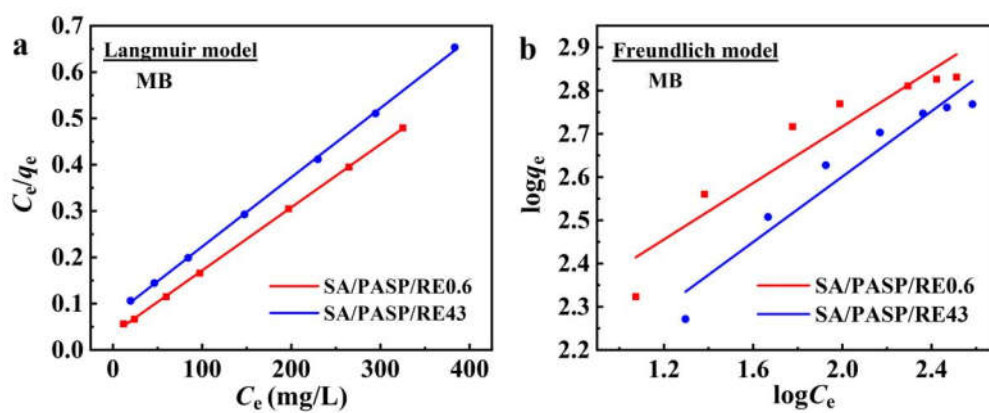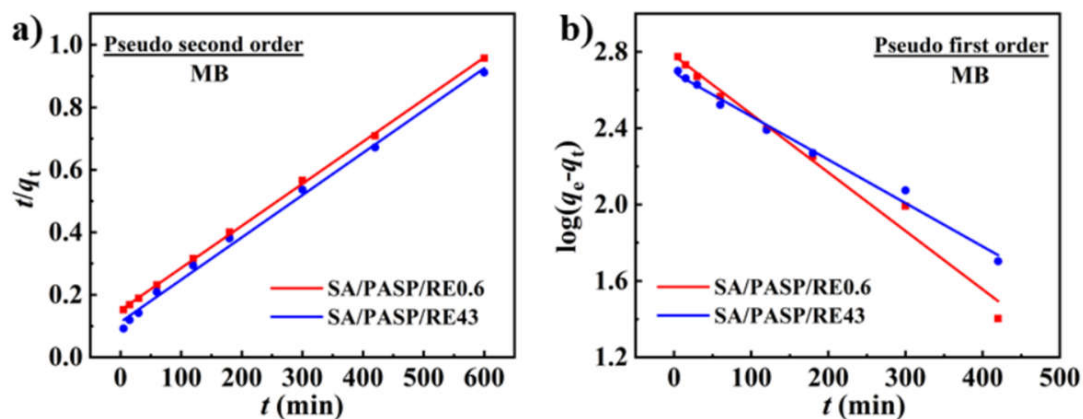

Figure S4. The linear fitting curves with Langmuir model (a) and the Freundlich model (b) for the adsorption of MB onto SA/PASP/RE0.6 and SA/PASP/RE43 beads.
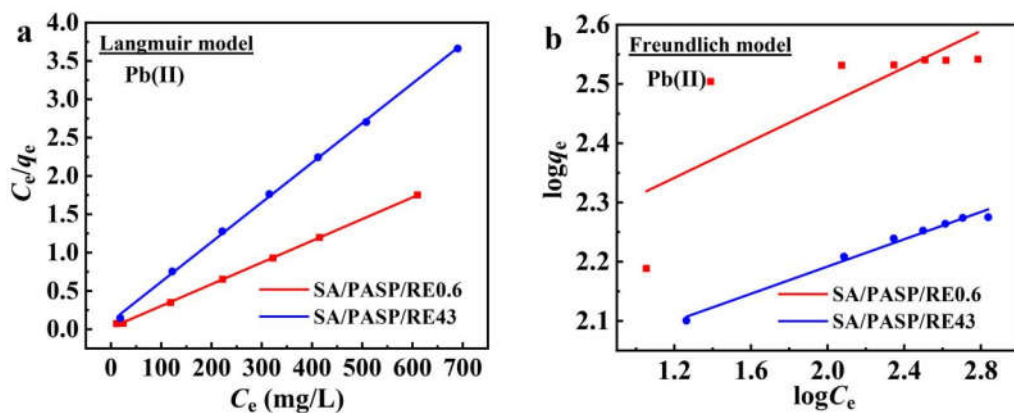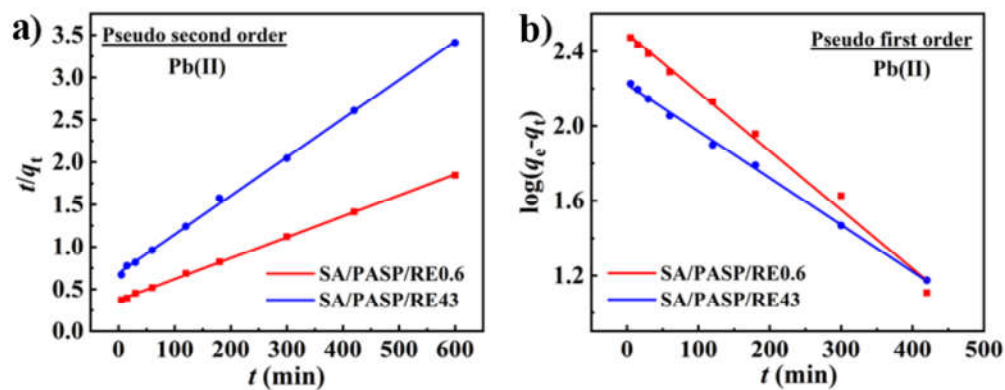
Figure S5. The linear fitting curves with Langmuir model (a) and the Freundlich model (b) for the adsorption of Pb(II) onto SA/PASP/RE0.6 and SA/PASP/RE43 beads.
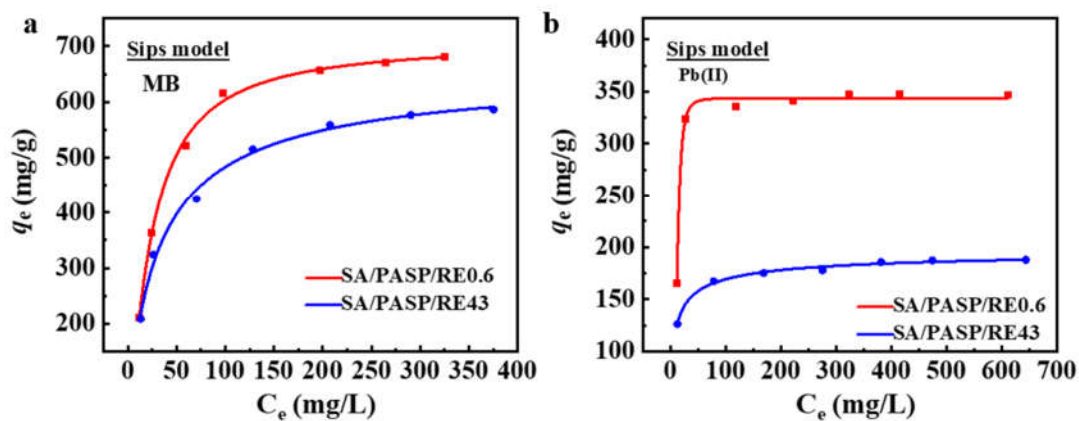
Figure S6. The nonlinear fitting curves with Sips model for the adsorption of MB (a) and Pb(II) (b) onto SA/PASP/RE0.6 and SA/PASP/RE43 beads.

Figure S7. The linear fitting curves with pseudo-second order (a) and pseudo-first order (b) kinetic models for the adsorption of MB onto the SA/PASP/RE0.6 and SA/PASP/RE43 beads.

Figure S8. The linear fitting curves with pseudo-first order (a) and pseudo-second order (b) kinetic models for the adsorption of Pb(II) onto the SA/PASP/RE0.6 and SA/PASP/RE43 beads.
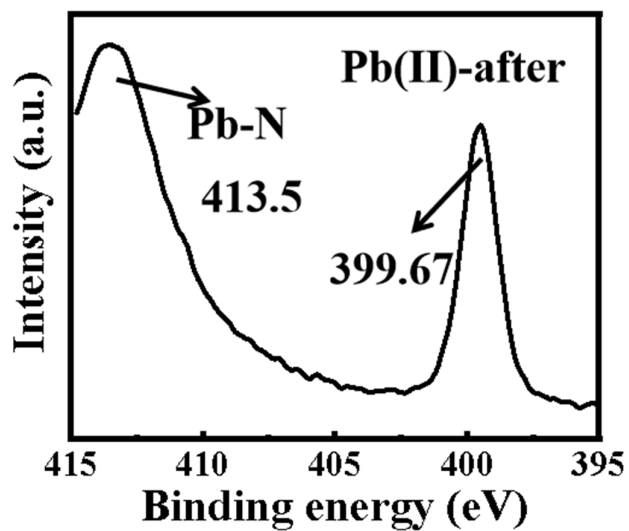
Figure S9. N1s spectra before and after adsorption of Pb(II).

Part III. Supplementary Tables

Table S1. Two-parameter adsorption model of the adsorption of MB and Pb(II) onto the composite beads.

Adsorbates	Samples	Langmuir			Freundlich		
		K_L(L/mg)	Q_m (mg/g)	R^2	K_F (L/mg)	n	R^2
MB	SA/PASP/RE0.6	0.035	735.29	0.9997	2.064	3.06	0.8942
	SA/PASP/RE43	0.073	666.67	0.9995	1.844	1.28	0.9362
Pb(II)	SA/PASP/RE0.6	0.021	353.36	0.9996	2.156	6.46	0.5243
	SA/PASP/RE43	0.102	193.05	0.9992	1.961	8.69	0.9826

Table S2. Three-parameter adsorption model of the adsorption of MB and Pb(II) onto the composite beads.

Adsorbates	Samples	Sips			
		Ks(L/g)	βs	as(L/mg)	R2
MB	SA/PASP/RE0.6	14.8425	1.2211	0.0209	0.9977
	SA/PASP/RE43	36.1505	0.8465	0.0545	0.9943
Pb(II)	SA/PASP/RE0.6	0.1151	1.3266	0.0003	0.9959
	SA/PASP/RE43	85.955	0.8533	0.4296	0.9932

Table S3. Adsorption kinetic parameters for the adsorption of MB and Pb(II) ions onto the composite beads.

Adsorbates	Samples	Pseudo-first-order model			Pseudo-second order model		
		$K_1 \times 10^2$ (min^{-1})	$q_{e,cal,1}$ (mg/g)	R^2	$K_2 \times 10^5$ (min^{-1})	$q_{e,cal,2}$ (mg/g)	R^2
MB	SA/PASP/RE0.6	0.0070	602.56	0.9790	1.24	729.93	0.9995
	SA/PASP/RE45	0.0052	489.33	0.9921	0.99	636.94	0.9965
Pb(II)	SA/PASP/RE0.6	0.0073	309.03	0.9926	1.64	404.86	0.9996
	SA/PASP/RE45	0.0058	165.96	0.9984	3.01	219.30	0.9991

References

[77] Ho, Y.S.; McKay, G. A comparison of chemisorption kinetic models applied to pollutant removal on various sorbents. *Process Saf. Environ.* **1998**, *76*, 332-340.

[78] Al-Ghouti, M.A.; Da'ana, D.A. Guidelines for the use and interpretation of adsorption isotherm models: A review. *J. Hazard. Mater.* **2020**, *393*, 122383.

[79] Fernandes, E.P.; Silva, T.S.; Carvalho, C.M.; Selvasembian, R.; Chaukura, N.; Oliveira, L.M.T.M.; Meneghetti, S.M.P.; Meili, L. Efficient adsorption of dyes by γ-alumina synthesized from aluminum wastes: Kinetics, isotherms, thermodynamics and toxicity assessment. *J. Environ. Chem. Eng.* **2021**, *9*, 106198.

[80] Deng, J.L.; Yang, L.L.; Liang, G.Z. Preparation, characterization and swelling behaviors sodium alginate-graft-acrylic acid/Na$^+$ rectorite superabsorbent composites. *J. Inorg. Organomet. Polym. Mater.* **2013**, *23*, 525-532.